Downlink Performance of Optical OFDM in Outdoor Visible Light Communication

BORJA GENOVÉS GUZMÁN[1]**, (Student Member, IEEE),**
VÍCTOR P. GIL JIMÉNEZ[1]**, (Senior Member, IEEE), MARI CARMEN AGUAYO-TORRES**[2]**,**
HARALD HAAS[3]**, (Fellow, IEEE), AND LAJOS HANZO**[4]**, (Fellow, IEEE)**

[1]Department of Signal Theory and Communications, Universidad Carlos III de Madrid, 28911 Madrid, Spain
[2]Communications Engineering Department, Universidad de Málaga, 29071 Málaga, Spain
[3]LiFi Research and Development Centre, School of Engineering, Institute for Digital Communications, The University of Edinburgh, Edinburgh EH8 9YL, U.K.
[4]School of Electronics and Computer Science, University of Southampton, Southampton SO17 1BJ, U.K.

Corresponding author: Lajos Hanzo (lh@ecs.soton.ac.uk)

ABSTRACT Visible light communication (VLC) is a promising ubiquitous design alternative for supporting high data rates. Its application has been primarily oriented to indoor scenarios, but the proliferation of light-emitting diodes in the streets warrants its investigation in outdoor scenarios as well. This paper studies the feasibility of VLC in a conventional outdoor scenario, when optical orthogonal frequency division multiplexing techniques are employed. The presence of sunlight reduces the system's performance, hence sophisticated adaptive techniques must be applied. Closed-form expressions of the signal-to-noise ratio and of the mean cell data rate are derived and our simulations demonstrate their accuracy. Besides, the outage probability when adaptive modulation and coding schemes are employed is analytically expressed. It is shown that, when modulation bandwidth adaptation is carried out depending on the time of day and the illuminance from ambient light, the mean cell data rate is increased and the outage probability is reduced.

INDEX TERMS Background noise, optical orthogonal frequency division multiplexing (O-OFDM), outdoor, visible light communication (VLC).

I. INTRODUCTION

The increasing demand for ubiquitous wireless Internet access is gradually exhausting the existing radio-frequency (RF) resources [1]. To prevent the looming spectrum crunch, the research community is considering diverse new technologies operating in high-frequency bands, such as the millimeter-wave [2] and the visible light communication (VLC) band [3]. The VLC solutions rely on light-emitting diodes (LEDs) that are capable of supporting high data rates on the order of Gbps [4].

However, VLC solutions have been predominantly focused on indoor scenarios due to their susceptibility to sunlight-induced shot noise. As a benefit, their security was improved, because the propagation of light was confined to a room. In indoor scenarios the number of LED light fixtures is high and the VLC attocells can be readily spotted based on their bright light-cone. Thus, user-centric VLC design is of great importance [5], [6]. Uplink (UL) RF technologies combined with downlink (DL) VLC define a hybrid system that substantially improves the network capacity [7], [8]. More explicitly, VLC and RF technologies complement each other, because the latter guarantees ubiquitous connectivity, while VLC supports high data rates due to its high signal-to-noise ratio (SNR) in the DL when a line-of-sight (LoS) link exists [9].

The solid state lighting technology is gradually also replacing the halogen lighting in outdoor scenarios. Hence we witness a proliferation of scenarios capable of transmitting information by means of light: LED boards, street lights, traffic lights, head lights, etc. The number of these scenarios
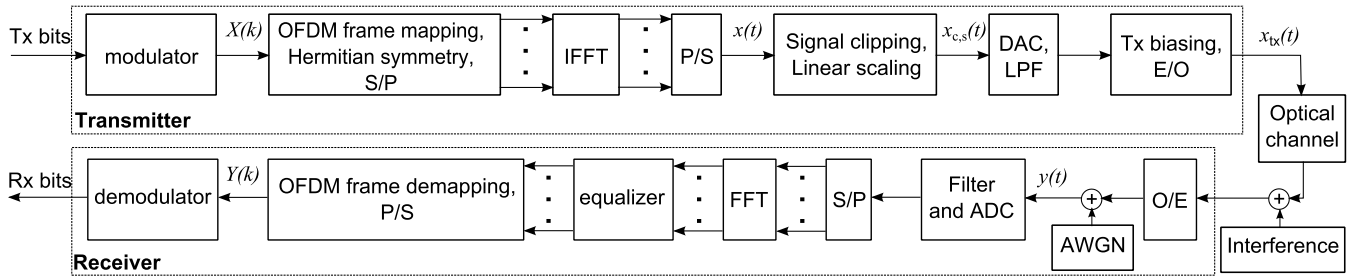
FIGURE 1. O-OFDM system.

is increasing, which may lead to the vision of a smart city, where all these sources provide Internet access. This fact opens the door for research studies of VLC techniques in outdoor scenarios.

Optical Wireless Communications (OWC) have been used in long-range systems for outdoor applications such as inter-building communications, last mile access networks [10], high altitude platform based laser communications and satellite communications [11]. These free-space optical (FSO) scenarios are often modeled as Gamma-gamma [12] or a lognormally distributed fading scenarios [13]. Uysal *et al.* presented a performance study of a vehicle-to-vehicle (V2V) and vehicle-to-infrastructure (V2I) communications system in [14]. They highlighted the challenges imposed by outdoor environments, such as severe weather conditions, sunlight and ambient light. The authors of [15] characterized the noticeable difference between the indoor and outdoor VLC channels. Explicitly, outdoor VLC has multiple dominant LoS links, but less reflected multipath components. Căilean and Dimian [16] addressed the challenges related to VLC when it is used in vehicular communications applications.

Outdoor VLC applications are bound to experience unmodulated parasitic light impinging on the photodetector (PD). The resultant direct-current (DC) component may be mitigated by capacitive filters, but it still results in strong shot noise, which would often inflict outages. In order to mitigate the background noise, Chung and Oh [17] invoked efficient optical filtering, whereas Lee *et al.* [18] designed a selective combining receiver. As a further solution, Kinoshita *et al.* [19] employed an image sensor as their reception device instead of a conventional PD. Knobloch [20] disseminated his experimental frame error rate (FER) results measured in a street lighting aided scenario, where pulse-width modulation (PWM) was used. Islim *et al.* [21] disseminated the first experimental study of the impact of solar irradiance on VLC and demonstrated its viability in such an environment.

Against this background, our main contribution is that we quantify the average data rate and optimize the modulation bandwidth, depending on the sunlight- and skylight-induced performance degradation, when a multicarrier transmission scheme is used. Therefore, the optimum modulation bandwidth will vary depending on the time of the day. This system

can rely on any LED access point (AP) located in outdoor scenarios, such as street lights, LED boards at railway stations, etc. Analytical SNR expressions are derived and the performance of the system is evaluated in terms of the average cell data rate and the outage probability, when adaptive modulation and coding (AMC) schemes are employed. Since the AP density is typically lower than in indoor scenarios and the predominant noise source in outdoor scenarios is the background noise, a single-cell scenario is studied. The back-haul network is assumed to be capable of managing all the traffic at high data rates. The UL is not analysed, because it relies on RF communications. The future popularity of the VLC technology in outdoor scenarios critically depends on its ability to cope with the multiple sources of parasitic light, which motivates the research presented in this treatise.

This paper is organized as follows. In Section II the system model is presented, where both the communications scenario and the AMC schemes used are described. Section III discusses the metrics relied upon for characterising the performance of the system. Our results are discussed in Section IV. Finally, our conclusions are offered in Section V.

II. SYSTEM MODEL

Fig. 1 illustrates the system model considered in this study. The input bits are mapped to quadrature amplitude modulated (QAM) symbols of an M-ary constellation. The AMC scheme utilized will be discussed in Section II-C. Suffice to say here that M varies according to the channel conditions quantified by the SNR. A set of K symbols are mapped to K frequency-domain (FD) subcarriers of either a direct current optical orthogonal frequency division multiplexing (DCO-OFDM) or of an asymmetrically clipped optical-OFDM (ACO-OFDM) scheme [22]. In the DCO-OFDM, $K/2 - 1$ symbols are mapped onto the first half of FD subcarriers, leaving the first FD subcarrier set to zero and the information is sent in the rest of the subcarriers having indices of $k = 1, 2, ..., K/2 - 1$. In the ACO-OFDM, $K/4$ symbols are mapped onto the first half of the odd FD subcarriers with indices of $k = 1, 3, ..., K/2 - 1$, leaving the even subcarriers set to zero. In both schemes, the information in the FD subcarrier $K/2$ is set to zero and the information transported on the second half of the FD subcarriers (with indices from $K/2 + 1$ to $K - 1$) are Hermitian symmetric

with respect to the information conveyed in the first half (with indices from 1 to $K/2 - 1$). This arrangement allows us to obtain a real-valued output signal $x(t)$ in the time domain (TD) after the inverse fast Fourier transform (IFFT).

The TD signal $x(t)$ must be clipped and scaled in order to constrain it to the dynamic range of the LED, resulting in $x_{c,s}(t) = \sigma_x V[x(t)]$, where σ_x is the electrical signal variance and $V[x(t)]$ represents the clipped signal defined as

$$V[x(t)] = \begin{cases} \lambda_t & : x(t) > \lambda_t \\ x(t) & : \lambda_t \geq x(t) \geq \lambda_b, \\ \lambda_b & : x(t) < \lambda_b \end{cases} \quad (1)$$

where λ_b and λ_t are the normalized TD bottom and top clipping levels, respectively. A certain illumination level and a minimum signal clipping are guaranteed thanks to the DC-bias I_{DC}. The optical TD transmitted signal can be written as

$$x_{tx}(t) = \eta_{led}\left[x_{c,s}(t) + I_{DC}\right], \quad (2)$$

where η_{led} is the electrical-to-optical conversion efficiency of the LED. Because of the TD differences of the signals transmitted by DCO-OFDM and ACO-OFDM, the scaling factor σ_x and the DC-bias I_{DC} are different. A larger I_{DC} value is needed for DCO-OFDM in order to shift the TD signal to the middle of the LED's dynamic range, whereas a minimum of I_{DC} is needed for ACO-OFDM with the only goal of guaranteeing the required illumination level. The beneficial values of these parameters will be studied in Section IV.

Considering a single-cell scenario, where no interference arrives from other APs, the TD received signal can be written as

$$y(t) = \eta_{pd}\left[x_{tx}(t) \circledast h(t)\right] + n_{Rx}(t), \quad (3)$$

where η_{pd} is the responsivity of the PD and $n_{Rx}(t)$ is the receiver noise in the TD, which obeys the zero-mean Gaussian distribution with variance σ_{Rx}^2. The channel impulse response (CIR) of the VLC system is denoted as $h(t) = \mathcal{F}^{-1}\{H(k)\}$, which has a frequency domain channel transfer function (FDCHTF) of $H(k)$ influenced both by the front-end devices (LED and PD) and by the free space transmission, formulated as

$$|H(k, r, W)| = |H_{fe}(k, W)| \cdot |H_{fs}(r)|, \quad (4)$$

where r is the horizontal distance between the AP and the receiver illustrated in Fig. 2, while W is the modulation bandwidth.

The FDCHTF of the front-end devices is modeled as [23]

$$|H_{fe}(k, W)| = \sqrt{\exp\left(-\frac{kW}{KF_{fe}}\right)}, \quad (5)$$

where F_{fe} is the so-called bandwidth factor that controls the FD characteristics. Thus, the limited modulation bandwidth of VLC systems is explicitly considered in this equation. The effect of the front-end devices at the receiver may be mitigated by using a cyclic prefix (CP), but it is beyond
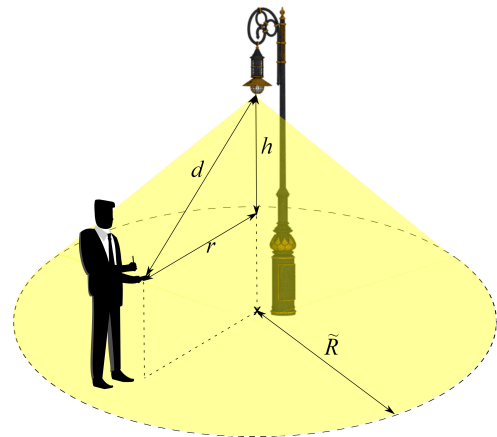

FIGURE 2. AP radiating.

the scope of this work. The free-space channel gain can be represented as [24]

$$|H_{fs}(r)| = \left|\frac{A_{pd}(m+1)h^{m+1}}{2\pi\left(r^2 + h^2\right)^{\frac{m+3}{2}}}\right|, \quad (6)$$

where the PD's physical area is given by A_{pd}, and h is the vertical separation between the AP and the PD. The Lambertian emission order of the LED is represented by m and a 90° receiver field of view is assumed, which means that all the users within the cell area can receive data from the AP.

The users are assumed to be uniformly distributed in the circular cell, hence we have $f_R(r) = \frac{2r}{\tilde{R}^2}$, where $\tilde{R}$ is the cell radius. The probability density function of the distance d between the AP and the PD is obtained by invoking the variable change of $d^2 = r^2 + h^2$, yielding

$$f_D(d) = \frac{2d}{\tilde{R}^2}, \qquad d \in \left[h, \sqrt{h^2 + \tilde{R}^2}\right]. \quad (7)$$

Typically a CP is inserted in OFDM systems in order to combat the intersymbol interference (ISI). However, the CP is not included in Fig. 1, because it may be deemed negligible in outdoor VLC systems exhibiting a low dispersion, when the SNR and throughput requirements are studied [25]. Likewise, the non-linearity of the LED's transfer function can be omitted, if pre-distortion methods are used for compensating the non-linear LED effects [26] or peak-to-average power ratio (PAPR) reduction techniques are invoked [27]. For this reason, a limited linear dynamic range is considered in this work.

A. OUTDOOR VLC
At the time of writing, VLC has been predominantly studied in indoor environments because of the high density of light fixtures and as a benefit of the reduced background light coming from natural sources. However, VLC has a potential also in outdoor scenarios in the smart cities of the near future. Many of the techniques proposed for indoor VLC are less applicable to outdoor VLC owing to the following reasons:

- *Scenario*: The heights of the APs and receivers, as well as the coverage area are rather different. The VLC coverage area in outdoor scenarios should ideally be larger than that in indoor ones. The atto-cell radius $\tilde{R}$ of indoor scenarios is typically around 2-3 m, whereas outdoors it is thought to be approximately 7 m if street lights are used. Furthermore, street lights are typically at the height of 8 m, whereas the indoor light fixture height is around 3 m. The users in indoor scenarios are typically seated at a desk having a height of approximately 0.75 m, whereas the outdoor users are likely to be standing, holding a communicator at the height of 1.20 m.
- *Illumination requirements*: Although they depend on the activity performed, the illumination requirements of indoor scenarios are more strict than the ones for outdoor. Typical values of cell center illuminance in indoor places are hundreds of lux (around 500 lux), while tens of lux are normal values for exterior scenarios. However, the optical transmit power is higher in outdoor scenarios because the street lights have to cover a larger area.
- *Ambient noise*: The contaminating illuminance in indoor scenarios is a few hundred lux, whereas in outdoor scenarios it is tens of thousands of lux. Hence, the outdoor receiver might be 'blinded'.
- *Shadowing*: The LoS link's blockage in VLC is one of its main drawbacks. In indoor scenarios, the LoS link's blockage probability increases due to the presence of people and furniture. Hence, cooperative user-centric AP-grouping [5], [6] techniques may have to be invoked for guaranteeing at least one LoS link with one AP [28], [29]. By contrast, the LoS link's blockage probability is reduced in outdoor scenarios due to the higher elevation of the AP and owing to the absence of furniture and extra obstacles.
- *Interference*: Although a wider variety of LEDs can be found in outdoor scenarios (heterogeneous scenario), the interference is expected to be lower than in indoor scenarios, because the cells are likely to be one-dimensional along a street, for example, which can be readily mitigated by using only two orthogonal frequency slots. The density of APs is much lower than in indoor environments.
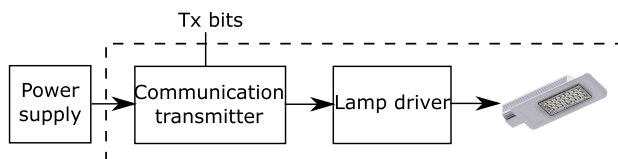

FIGURE 3. Block diagram for the VLC transmitter.

Fig. 3 represents the block diagram of the VLC transmitter that can be used for implementing the system. To convert a traditional street-light into a VLC transmitter that provides simultaneous illumination and communication, a "communication transmitter" must be installed. It receives the

information to be transmitted and carries out the task of coding and modulation before being superimposed on the electrical signal of the LED lamp. The lamp driver is required for managing the alternating current to direct current (AC/DC) conversion in an energy efficient way (dimming mode if desired) and without causing any temperature problem. The dashed-line rectangle represents the transmitter of Fig. 1, which is composed by the communication transmitter module and the LED lamp.
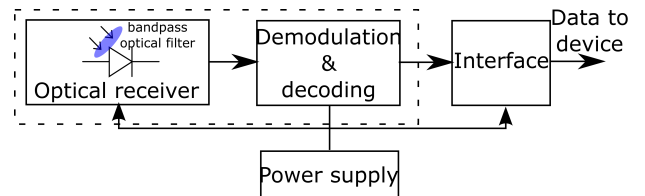

FIGURE 4. Block diagram for the VLC receiver.

At the receiver side of Fig. 4, we find the optical receiver composed of a bandpass optical filter and a PD for converting the optical signal to electrical signal, including the transimpedance amplifier (TIA). Next, we can observe the demodulation and decoding block provided for detecting data. Finally, the receiver has an interface block whose function is to send the data to an external device, such as a PC or a smart-phone. All these modules must be powered adequately. Again, the dashed-line rectangle represents the receiver side of Fig. 1.

The transmitter may rely on well-known manufacturers' lamps, which include drivers capable of powering multiple LEDs and they can be modulated simultaneously.

B. OPTICAL OFDM TECHNIQUES

A pair of Optical-OFDM (O-OFDM) techniques are studied in this paper, namely DCO-OFDM and ACO-OFDM. The FD subcarriers employed for carrying useful information are different in these modulation schemes, whose indices are represented as $\mathcal{K}_{\text{DCO}} = \{1, 2, 3, ..., K/2 - 1\}$ and $\mathcal{K}_{\text{ACO}} = \{1, 3, 5, ..., K/2 - 1\}$ for DCO-OFDM and ACO-OFDM schemes, respectively. To jointly represent $\mathcal{K}_{\text{DCO}}$ and $\mathcal{K}_{\text{ACO}}$, they are expressed as $\mathcal{K}_*$. These schemes exhibit different characteristics, when their clipping distortion is considered.

The Bussgang theorem is used for modelling the non-linearly clipped TD signal $V[x(t)]$ of (1) as [30]

$$V_{\text{DCO}}[x(t)] = \rho x(t) + n_{\text{clip}}(t), \tag{8}$$

$$V_{\text{ACO}}[x(t)] = 2U[x(t)]\rho x(t) + n_{\text{clip}}(t), \tag{9}$$

where $U[x(t)]$ is the unit-step function, $n_{\text{clip}}(t)$ is the clipping noise sample in the TD and ρ is an attenuation factor related to the clipping effect that can be approximated as $\rho = Q(\lambda_{\text{b}}) - Q(\lambda_{\text{t}})$, where $Q(x)$ is the well-known Gaussian Q-function. Again, the clipping effects are different for DCO-OFDM and ACO-OFDM. As a consequence, the parameters ρ and $n_{\text{clip}}(t)$ also differ. In DCO-OFDM and

ACO-OFDM, the electrical transmitted power used for communication (without DC-value) is represented by the same equation

$$P_{\text{elec}} = \eta_{\text{led}}^2 \sigma_{\text{x}}^2 \left(\rho^2 + \sigma_{\text{clip}}^2 \right). \tag{10}$$

Thus, the SNR equations of the DCO-OFDM and ACO-OFDM scenarios are both given by

$$\Gamma(k, r, W) = \frac{\eta_{\text{pd}}^2 \eta_{\text{led}}^2 \sigma_{\text{x}}^2 \rho^2 \xi^2 \, |H(k, r, W)|^2}{\eta_{\text{pd}}^2 \eta_{\text{led}}^2 \sigma_{\text{x}}^2 \sigma_{\text{clip}}^2 \, |H(k, r, W)|^2 + \sigma_{\text{Rx}}^2(W)}, \tag{11}$$

where $H(k, r, W)$ is the FDCHTF of the VLC channel on the k-th FD subcarrier, r is the horizontal distance (see Fig. 2) and W is the modulation bandwidth. In order to make a fair comparison, since some FD subcarriers do not carry energy, a normalization factor ξ is needed so that both transmit powers are the same. In the case of DCO-OFDM, the FD subcarriers 0 and K/2 do not carry energy, while in the case of ACO-OFDM all the even subcarriers are zero. Given the total number of FD subcarriers K, the associated normalization factor is given by

$$\xi_{\text{DCO}} = \sqrt{K/(K-2)} \tag{12}$$

and

$$\xi_{\text{ACO}} = \sqrt{2K/K} \tag{13}$$

for DCO-OFDM and ACO-OFDM, respectively. The optical transmitted power is computed as

$$P_{\text{opt}} = E[x_{\text{tx}}(t)] = \eta_{\text{led}} \left(\sigma_{\text{x}} E[V(x(t))] + I_{\text{DC}} \right). \tag{14}$$

It was shown in [30] that $V[x(t)]$ follows a truncated Gaussian distribution and its mean can be calculated using its statistics [31] as $E[V(x(t))] = f_N(\lambda_{\text{b}}) - f_N(\lambda_{\text{t}}) + \lambda_{\text{t}} Q(\lambda_{\text{t}}) + \lambda_{\text{b}}[1 - Q(\lambda_{\text{b}})]$. From (14), the electrical signal variance σ_{x}^2 is derived as

$$\sigma_{\text{x}}^2 = \frac{P_{\text{opt}}^2}{\eta_{\text{led}}^2 \left(\zeta + E[V(x(t))] \right)^2} = \frac{\left(\frac{2\pi E_{\text{V}} h^2}{(m+1) K_{\text{e/v}}} \right)^2}{\eta_{\text{led}}^2 \left(\zeta + E[V(x(t))] \right)^2}, \tag{15}$$

where the parameter E_{V} represents the illuminance in the area right below the LED, which is also referred to as the illuminance at the cell center, $K_{\text{e/v}}$ is the luminous efficacy and $\zeta = \frac{I_{\text{DC}}}{\sigma_{\text{x}}}$ is defined as the ratio of DC-bias level to the electrical signal's standard deviation. The variable P_{opt} in (15) is derived from the calculation of the cell center illuminance as $E_{\text{v}} = Q \cdot \frac{H_{\text{fs}}(0)}{A_{\text{pd}}}$, where Q is the output luminous flux of the LED expressed in lm (= lx · m²), that can be written as $Q = K_{\text{e/v}} \cdot P_{\text{opt}}$ and $H_{\text{fs}}(0)$ is the free-space channel gain between the AP and the cell center where $r = 0$, calculated as (6).

At the receiver, the FFT is used for demodulation, where the clipping noise component is assumed to be Gaussian distributed according to the central limit theorem (CLT), with

zero mean and a variance of σ_{clip}^2 [30], [32]. Using the statistics of a truncated Gaussian distribution, σ_{clip}^2 is expressed in DCO-OFDM as [30]

$$
\begin{aligned}
\sigma_{\text{clip,DCO}}^2 \\
&= Q(\lambda_{\text{b}}) - Q(\lambda_{\text{t}}) + f_N(\lambda_{\text{b}})\lambda_{\text{b}} - f_N(\lambda_{\text{t}})\lambda_{\text{t}} \\
&\quad + [1 - Q(\lambda_{\text{b}})] \lambda_{\text{b}}^2 + Q(\lambda_{\text{t}})\lambda_{\text{t}}^2 - \rho^2 \\
&\quad - [f_N(\lambda_{\text{b}}) - f_N(\lambda_{\text{t}}) + [1 - Q(\lambda_{\text{b}})] \lambda_{\text{b}} + Q(\lambda_{\text{t}})\lambda_{\text{t}}]^2, \tag{16}
\end{aligned}
$$

whereas in ACO-OFDM it becomes

$$
\begin{aligned}
\sigma_{\text{clip,ACO}}^2 &= -2\rho^2 + 2f_N(\lambda_{\text{t}})\lambda_{\text{b}} - f_N(\lambda_{\text{t}})\lambda_{\text{t}} - f_N(\lambda_{\text{b}})\lambda_{\text{b}} \\
&\quad + (\lambda_{\text{b}}^2 + 1) [Q(\lambda_{\text{b}}) - Q(\lambda_{\text{t}})] + Q(\lambda_{\text{t}})(\lambda_{\text{t}} - \lambda_{\text{b}})^2. \tag{17}
\end{aligned}
$$

Additionally, the receiver noise variance is formulated as

$$
\begin{aligned}
\sigma_{\text{Rx}}^2(W) &= \frac{N_0 W}{\xi^2} = \frac{\left(N_{0,\text{s}} + N_{0,\text{ab}} + N_{0,\text{tn}} \right) W}{\xi^2} \\
&= \frac{\left(2q P_{\text{opt,Rx}} \eta_{\text{pd}} + 2q E_{\text{r,ab}} A_{\text{pd}} \eta_{\text{pd}} + \frac{4\kappa_{\text{B}} T}{R_{\text{L}}} \right) W}{\xi^2}, \tag{18}
\end{aligned}
$$

where $N_{0,\text{s}}$, $N_{0,\text{ab}}$ and $N_{0,\text{tn}}$ represent the power spectral density (PSD) of the shot noise, the noise produced by the ambient light and the thermal noise, respectively. The incident irradiance in the outdoor environment is represented by

$$E_{\text{r,ab}} = \int_{\Lambda_1}^{\Lambda_2} P_{\text{S}}(\Lambda) \cdot T_{\text{f}}(\Lambda) \, d\Lambda, \tag{19}$$

where $P_{\text{S}}(\Lambda)$ is the solar spectral irradiance and $T_{\text{f}}(\Lambda)$ is the transmittance of the optical bandpass filter from wavelength Λ_1 to Λ_2 in the event that one is utilized. The charge of an electron is $q = 1.6 \cdot 10^{-19}$ C, the Boltzmann constant is $\kappa_{\text{B}} = 1.38 \cdot 10^{-23}$ J/K, the absolute temperature is denoted by T and finally R_{L} is the load resistance in the receiver circuit. Note that the receiver noise σ_{Rx}^2 depends on the modulation bandwidth W. The optical received power is given by

$$P_{\text{opt,Rx}}(r) = P_{\text{opt}} H_{\text{fs}}(r) = \frac{2\pi E_{\text{V}} h^2}{(m+1) K_{\text{e/v}}} \cdot \frac{A_{\text{pd}}(m+1) h^{m+1}}{2\pi \left(r^2 + h^2 \right)^{\frac{m+3}{2}}}, \tag{20}$$

where r denotes the horizontal distance between the AP and the user.

By appropriately combining Equations (1)-(20), the SNR may be expressed as

$$\Gamma(k, d, W) = \frac{C_1}{C_4 + \left(C_2 \cdot d^\alpha + C_3 \cdot d^{2\alpha} \right) \cdot W \cdot \exp\left(\frac{kW}{KF_{\text{fe}}} \right)}, \tag{21}$$

where we have

$$C_1 = \left(\eta_{\text{pd}} E_{\text{V}} h^{m+3} A_{\text{pd}} \xi^2 \rho \right)^2 \tag{22}$$

$$C_2 = 2q E_{\text{V}} K_{\text{e/v}} \left(\zeta + E[V(x(t))] \right)^2 A_{\text{pd}} h^{m+3} \eta_{\text{pd}} \tag{23}$$

$$C_3 = \left(2q E_{\text{r,ab}} A_{\text{pd}} \eta_{\text{pd}} + \frac{4\kappa_{\text{B}} T}{R_{\text{L}}} \right) K_{\text{e/v}}^2 \left(\zeta + E[V(x(t))] \right)^2 \tag{24}$$

$$C_4 = \left(\eta_{\mathrm{pd}} E_{\mathrm{V}} h^{m+3} A_{\mathrm{pd}} \xi \, \sigma_{\mathrm{clip}} \right)^2 \tag{25}$$

$$\alpha = m + 3. \tag{26}$$

Note that as expected, the SNR $\Gamma(k, d, W)$ decreases with the distance d between the LED and the PD (see Fig. 2), as well as with the modulation bandwidth W. Furthermore, the higher the index k of a FD subcarrier, the lower the SNR becomes due to the FDCHTF shape of the front-end devices formulated in (5).

C. ADAPTIVE MODULATION AND CODING

The Shannon limit of the continuous-input continuous-output memoryless channel (CCMC) is represented by the well-known capacity expression of

$$\eta_s = \log_2(1 + \Gamma), \tag{27}$$

with Γ denoting the signal-to-interference-plus-noise ratio (SINR) at the receiver, or the SNR in a single-cell scenario. The cumulative density function (CDF) of the CCMC capacity can be written as

$$F_{\eta_s}(x) = \Pr\{\eta_s < x\} = F_{\Gamma}(2^x - 1), \tag{28}$$

where $F_{\Gamma}(\gamma)$ is the CDF of the SINR.

In practice, only certain discrete throughput modems can be used, hence the associated discrete-input continuous-output memoryless channel (DCMC) capacity can be achieved [33]. Explicitly, in AMC the range of SINRs is divided into $(N+1)$ channel quality regions $\Re_n = \{\gamma_{\mathrm{th}}[n], \gamma_{\mathrm{th}}[n + 1]\}$, $n = 0, 1, ..., N$ with $\gamma_{\mathrm{th}}[0] = 0$ and $\gamma_{\mathrm{th}}[N + 1] = \infty$. Within the channel quality region $\Re_n$, a certain constellation/coding scheme associated with $\epsilon[n]$ bits/symbol is employed. Below $\gamma_{\mathrm{th}}[1]$ no transmission is activated and the system is said to be in outage. Over $\gamma_{\mathrm{th}}[N]$ no further increase in SINR improves the throughput attained.

The set of switching thresholds between the constellations $\{\gamma_{\mathrm{th}}[n]\}_{n=1,..,N}$ has to be designed to satisfy the bit error rate (BER) target of the system [33]. The AMC throughput can be written as a function of the SINR as

$$\eta_{AMC} = \epsilon[n], \quad \mathrm{SINR} \in [\gamma_{\mathrm{th}}[n], \gamma_{\mathrm{th}}[n + 1]]. \tag{29}$$

For a certain average SNR Γ, the average throughput under AMC can be expressed as

$$\begin{aligned} E\left[\eta_{AMC}\right] &= \sum_{n=1}^{N} \epsilon[n] \cdot \Pr\{\gamma_{\mathrm{th}}[n] \le \Gamma < \gamma_{\mathrm{th}}[n + 1]\} \\ &= \sum_{n=1}^{N} \epsilon[n] \cdot [F_{\Gamma}(\gamma_{\mathrm{th}}[n+1]) - F_{\Gamma}(\gamma_{\mathrm{th}}[n])]. \end{aligned} \tag{30}$$

III. SYSTEM PARAMETER EVALUATION
A. SNR STATISTICS
The CDF of the SNR in (21) evaluated in terms of γ_{th} can be expressed as

$$\begin{aligned} & F_{\Gamma}(\gamma_{\mathrm{th}}) \\ &= \Pr\{\Gamma(k, D, W) < \gamma_{\mathrm{th}}\} \end{aligned}$$

$$= \Pr\left\{ C_4 \gamma_{\mathrm{th}} + \left(C_2 D^{\alpha} + C_3 \, D^{2\alpha} \right) W \exp\left(\frac{kW}{KF_{\mathrm{fe}}} \right) \gamma_{\mathrm{th}} - C_1 > 0 \right\}$$

$$= \Pr\{D > d_{\mathrm{th}}(\gamma_{\mathrm{th}}, W, k)\}$$

$$= \int_{d_{\mathrm{th}}(\gamma_{\mathrm{th}}, W, k)}^{\sqrt{h^2 + \tilde{R}^2}} f_D(d) \, \mathrm{d}d = 1 + \frac{h^2 - d_{\mathrm{th}}^2(\gamma_{\mathrm{th}}, W, k)}{\tilde{R}^2}, \tag{31}$$

where

$$d_{\mathrm{th}}(\gamma_{\mathrm{th}}, W, k)$$

$$= \left(\frac{-C_2}{2C_3} + \sqrt{\left(\frac{C_2}{2C_3} \right)^2 + \frac{C_1 - C_4 \gamma_{\mathrm{th}}}{C_3 W \exp\left(\frac{kW}{KF_{\mathrm{fe}}} \right) \gamma_{\mathrm{th}}}} \right)^{1/\alpha},$$

$$d_{\mathrm{th}}(\gamma_{\mathrm{th}}, W, k) \in \left[h, \sqrt{h^2 + \tilde{R}^2} \right].$$

When AMC schemes are invoked, the outage probability is obtained from Equation (31) as

$$\begin{aligned} F_{\Gamma|k=1}(\gamma_{\min}) &= \Pr\{\Gamma(k = 1, D, W) < \gamma_{\min}\} \\ &= 1 + \frac{h^2 - d_{\mathrm{th}}(\gamma_{\min}, W, k = 1)}{\tilde{R}^2}, \end{aligned} \tag{32}$$

where $\gamma_{\min}$ corresponds to the minimum SINR required for having a non-zero throughput for the AMC scheme. Again, the higher the FD subcarrier index, the higher the FD attenuation in (5).

B. AVERAGE DATA RATE STATISTICS
The average data rate $s(W)$ can be expressed as a function of the bandwidth W.

1) SHANNON LIMIT
Here we assume the employment of 'perfect capacity-achieving coding'. Hence the attainable throughput can be formulated as

$$\begin{aligned} s(W) &= \frac{W}{K} \sum_{k \in \mathcal{K}_*} \mathrm{E}\left[\log_2 \left(1 + \Gamma(k, d, W) \right) \right] \\ &= \frac{W}{K} \sum_{k \in \mathcal{K}_*} \int_{h}^{\sqrt{h^2 + \tilde{R}^2}} \log_2 \left(1 + \Gamma(k, d, W) \right) f_D(d) \mathrm{d}d, \end{aligned} \tag{33}$$

where the factor $\frac{W}{K}$ represents the bandwidth of each FD subcarrier, and $\mathcal{K}_*$ is the set of FD subcarriers indices that carry useful information, depending on the choice of the ACO-OFDM or DCO-OFDM scheme.

2) AMC SCHEMES
When using AMC schemes for maximizing the performance attained according to the prevalent channel conditions, the average data rate is expressed as

$$s(W)$$

$$= \frac{W}{K} \sum_{k \in \mathcal{K}_*} \sum_{n=1}^{N} \epsilon[n] \Big(\Pr\left\{ \Gamma(k, d, W) < \gamma_{\mathrm{th}}[n + 1] \right\}$$

TABLE 1. System parameters.

Parameter	Value	Unit
Cell radius, $\tilde{R}$	7	[m]
AP height	8	[m]
PD height	1.20	[m]
Modulation bandwidth, W	5 to 360	[MHz]
Front-end device bandwidth factor, F_{fe}	31.7	[MHz]
Ratio DC-standard deviation ζ_{DCO}	5.05	[dB]
Ratio DC-standard deviation ζ_{ACO}	2.05	[dB]
PD responsivity, η_{pd}	0.4	[A/W]
PD physical area, A_{pd}	1	[cm^2]
Number of FD subcarriers, K	512	
Power reduction factor, σ_P	10	[dB]
Cell center illuminance from AP, E_V	40	[lux]
Sun luminous efficacy, η_{sun}	93	[lm/W]
Absolute temperature, T	300	[K]
Receiver load resistance, R_L	50	[Ω]

$$
\begin{aligned}
&- \Pr\{\Gamma(k, d, W) < \gamma_{\text{th}}[n]\}\Big)\\
&= \frac{W}{K} \sum_{k \in \mathcal{K}_*} \sum_{n=1}^{N} \epsilon[n] \left(\int_{d_{\text{th}}(\gamma_{\text{th}}[n+1], W, k)}^{\sqrt{h^2 + \tilde{R}^2}} \frac{2d}{\tilde{R}^2} \, \mathrm{d}d - \int_{d_{\text{th}}(\gamma_{\text{th}}[n], W, k)}^{\sqrt{h^2 + \tilde{R}^2}} \frac{2d}{\tilde{R}^2} \, \mathrm{d}d \right)\\
&= \frac{W}{K} \sum_{k \in \mathcal{K}_*} \sum_{n=1}^{N} \epsilon[n] \left(\frac{d_{\text{th}}^2(\gamma_{\text{th}}[n], W, k) - d_{\text{th}}^2(\gamma_{\text{th}}[n+1], W, k)}{\tilde{R}^2} \right).
\end{aligned}
\tag{34}
$$

When relying on 'perfect capacity-achieving coding' and AMC, the average data rate satisfies $\lim_{W \to \infty} s(W) = \lim_{W \to 0} s(W) = 0$, as demonstrated in the Appendix. Since $s(W)$ is a continuous function at every point of its FD W, there is an optimum W that maximizes s, leading to the maximal data rate.

IV. PERFORMANCE RESULTS

A single-cell scenario having a radius of $\tilde{R} = 7$ m, LED AP height of 8 m and PD height of 1.20 m is considered. This setup results in $h = 6.80$ m. The values of the different parameters are shown in Table 1. The modulation bandwidth is the specific parameter under study, and it can assume a value spanning from 5 to 360 MHz. The front-end devices utilized for this study are the same as in [34] and have a bandwidth factor of $F_{\text{fe}} = 31.7$ MHz to model their FDCHTF as in (5). Due to the zero-clipping carried out in ACO-OFDM, the DC-bias level necessary for shifting the TD signal to the centre of the LED's dynamic range is lower than that in DCO-OFDM. The authors of [30] conducted a study of the clipping noise effects in OFDM-based optical wireless communication. The normalized bottom and top clipping levels are selected to minimize the clipping noise: in DCO-OFDM, we use $\lambda_t = 3.2$ and $\lambda_b = -3.2$; whereas in ACO-OFDM, $\lambda_t = 3.2$ and $\lambda_b = 0$. Thus, the DC-bias level required is:

- In DCO-OFDM: $I_{\text{DC}} = \sigma_x \zeta_{\text{DCO}} = \sigma_x \lambda_{t, \text{DCO}} \Rightarrow \zeta_{\text{DCO}} = \lambda_{t, \text{DCO}} = -\lambda_{b, \text{DCO}} = 3.2 = 5.05$ dB.
- In ACO-OFDM: $I_{\text{DC}} = \sigma_x \zeta_{\text{ACO}} = \sigma_x \lambda_{t, \text{ACO}}/2 \Rightarrow \zeta_{\text{ACO}} = \lambda_{t, \text{ACO}}/2 = 1.6 = 2.05$ dB.

The power reduction factor (σ_P) is the dual pair of the pathloss in classical RF systems, which quantifies the ratio of the received optical power at the cell center and at the cell edge, and it is configured to be 10 dB in order not to cause much SNR difference among users within a cell. That is, a user located at the cell edge will exhibit 10 dB lower SNR compared to a user located at the cell center, as seen in Fig. 5. This difference in optical received power is determined by the Lambertian emission order m given by

$$
m = \frac{\ln \sigma_P}{\ln\left(1 + \frac{R^2}{h^2}\right)} - 3.
\tag{35}
$$

Furthermore, $K = 512$ FD subcarriers are used, along with $E_V = 40$ lux, $T = 300$ K and $R_L = 50\,\Omega$. The SPCTRAL2 simulation model [35] is utilized in our study to compute spectral irradiance measurements in a certain location. The Atacama desert (24°30'S 69°15'W) was selected as the worst-case location for this study, noting that in much of the world there is less daylight than in there [36]. The highest spectral irradiance in the Atacama desert occurs in December. Thus, data was generated for the 354$^{\text{th}}$ day of the year assuming a detector elevation angle of 0°. The phosphor-coated white LEDs suffer from a slow response produced by the phosphor yellow light component [23]. This bandwidth can be boosted by invoking a bandpass optical blue filter at the receiver. At the same time, it reduces the shot noise and the risk of receiver saturation. Thus, a Semrock (97% transmittance at 452 nm, 45 nm bandwidth) optical blue filter is utilized in our study. Depending on the time of the day, the incident irradiance after the optical blue filter ($E_{\text{r,ab}}$) can vary from 0 to 116.71 $\frac{\text{W}}{\text{m}^2}$ corresponding to night-time and noon, with illuminances from ambient light in the visible range ($E_{\text{v,ab,vr}}$) of 0 and 52622 lux, respectively. The illuminance from ambient light in the visible and the incident irradiance after the blue filter in the given location are represented in Table 2. The illuminance from ambient light after the optical blue filter ($E_{\text{v,ab}}$) is expressed as

$$
E_{\text{v,ab}} = E_{\text{r,ab}} \cdot \eta_{\text{sun}},
\tag{36}
$$

TABLE 2. Average illuminance from ambient light in the visible range and incident irradiance after blue filter throughout the day.

Time of day	6h	7h	8h	9h	10h	11h	12h	13h	14h	15h	16h	17h	18h
Illuminance, $E_{\text{v,ab,vr}}$, [lux]	1927	11525	23444	34542	43543	49716	52622	52061	48073	40931	31162	19616	7928
Irradiance after filter, $E_{\text{r,ab}}$, $\frac{\text{W}}{\text{m}^2}$	4.88	23.58	49.57	74.83	95.61	109.95	116.71	115.41	106.13	89.57	67.08	41.03	16.27

(a) SNR [dB] at DC at night $(E_{v,ab,vr}=0\,\mathrm{lux})$

(b) Illuminance [lux] at night $(E_{v,ab,vr}=0\,\mathrm{lux})$

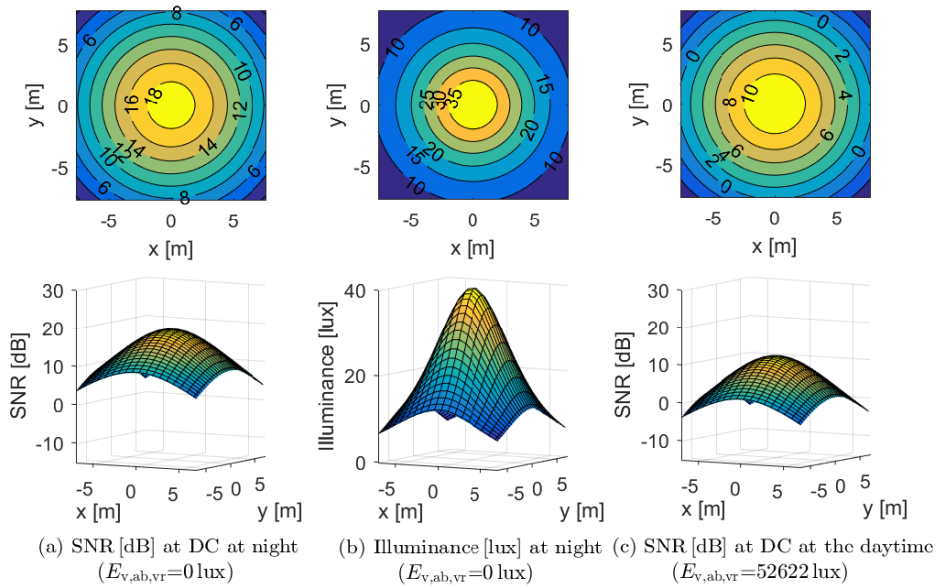(c) SNR [dB] at DC at the daytime $(E_{v,ab,vr}=52622\,\mathrm{lux})$

FIGURE 5. Single-cell scenario performance for $W = 360\,\mathrm{MHz}$, DCO-OFDM and different ambient conditions (2D: top, 3D: bottom).

where η_{sun} is the sun's luminous efficacy. These values result in an optical transmit power of $P_{opt} = 61.2\,\mathrm{W}$, which is a value within the typical ranges of commercial LED street lights [37].

The shot noise is the main noise in a VLC system in outdoor scenarios. Although the ambient light effect may be mitigated by means of filters owing to its slowly-varying DC-like nature, it still causes shot noise at the receiver front-ends. This effect can be seen in Fig. 5, where a difference of 7.5 dB is observed between the SNR at DC in a DCO-OFDM single-cell scenario at night (Fig. 5 (a)) and at the daytime using $E_{v,ab,vr} = 52622\,\mathrm{lux}$ and $W = 360\,\mathrm{MHz}$ (Fig. 5 (c)). The SNR in Fig. 5 refers to the SNR at DC over all the coverage area points, *i.e.*, the SNR for the subcarrier $k = 0$ and $W = 360\mathrm{MHz}$ is expressed as $\Gamma(k = 0, r, W = 360\mathrm{MHz})$ in (11). As (18) shows, the lower the sampling frequency, the lower the noise at the receiver becomes, which of course reduces the data rate achieved. Fig. 5 (b) represents the illuminance at night in the cell, where a cell center illuminance of $E_V = 40\,\mathrm{lux}$ is used according to the ANSI/IESNA RP-8-14 lighting regulation. In the case of Fig. 5 (a), communications become feasible. However, Fig. 5 (c) shows the difficulty of having a sufficiently high SNR for reliable communications during the daytime.

The CDF of the SNR at DC at night and during the daytime is depicted in Fig. 6. Again, there is an SNR loss of 7.5 dB during the daytime in comparison to the performance at night. The reason behind this is the shot noise produced at the receiver due to the ambient light. Furthermore, an SNR difference of 5 dB is observed between DCO-OFDM and ACO-OFDM. The reason for this is the fact that the receiver's noise variance in ACO-OFDM is about half that of the corresponding to DCO-OFDM, because almost
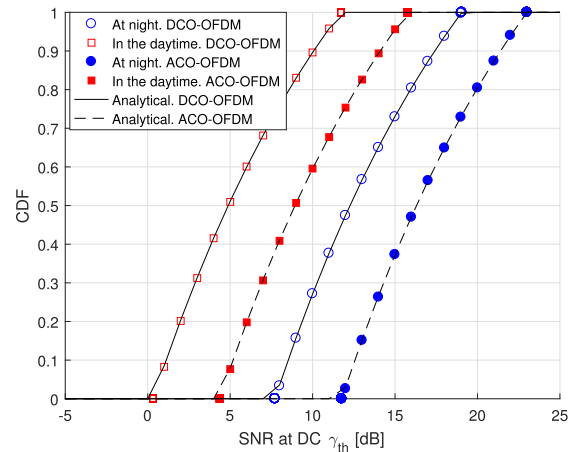

FIGURE 6. Cumulative Distribution Function of the SNR at FD subcarrier index $k = 0$ (DC) and at a $W = 360\,\mathrm{MHz}$ for different conditions. $F_{\Gamma}|_{k=0,W=360\,\mathrm{MHz}}(\gamma_{th})$.

half of the FD subcarriers $(K/2 - 1)$ carry useful information in DCO-OFDM, whereas only a quarter of them carry useful information in ACO-OFDM. Thus, according to (12) and (13), we have $\xi^2_{ACO} \approx 2\xi^2_{DCO}$ and as a consequence of (18), we have $\sigma^2_{Rx,ACO} \approx \sigma^2_{Rx,DCO}/2$. Furthermore, part of the electrical power in DCO-OFDM is wasted for the DC-bias, hence only part of it is used for communication, whereas ACO-OFDM needs much lower power for biasing and therefore more power is used for communications.

Section III-B demonstrated that the average data rate is a continuous function of W and there is a maximum in its domain of $W > 0$. Two different AMC schemes are investigated, whose operating regions are shown in Table 3.

TABLE 3. Adaptive modulation and coding SINR regions.

AMC$_1$			AMC$_2$			
$\gamma_{\text{th}}[n]$ [dB]	Modulation	$\epsilon[n]$ [bits/symbol]	$\gamma_{\text{th}}[n]$ [dB]	Modulation	Code rate	$\epsilon[n]$ [bits/symbol]
7.6 ($\gamma_{\min}$)	BPSK	1	5 ($\gamma_{\min}$)	16QAM	0.369	1.4766
9.8	QPSK	2	8	16QAM	0.476	1.9141
13.4	8QAM	3	9	16QAM	0.602	2.4063
16.5	16QAM	4	11	64QAM	0.455	2.7305
19.6	32QAM	5	12	64QAM	0.554	3.3223
22.5	64QAM	6	14	64QAM	0.650	3.9023
25.5	128QAM	7	16	64QAM	0.754	4.5234
28.4	256QAM	8	18	64QAM	0.853	5.1151
-	-	-	20	64QAM	0.926	5.5547

The AMC$_1$ scheme corresponds to uncoded QAM [38] and the regions are configured for a BER = 10^{-3}, while AMC$_2$ is more spectrally efficient than AMC$_1$ and it is reminiscent of the 4G in the Long Term Evolution scheme [39], where a cyclic redundancy check (CRC) and turbo-coding are utilized. The SINR regions of AMC$_2$ are not standardized and then they depend on the operator. The ones here utilized are obtained from [39]. The analytical expressions of the average data rate were obtained in (33) and (34), where the CCMC capacity or realistic AMC schemes were assumed, respectively. These analytical curves are plotted using continuous or dashed lines in Fig. 7 and Fig. 8, during the daytime and at night, respectively, together with our simulation results represented by symbols. Note that the simulations closely match the analytical curves, which confirms the accuracy of our analytical expressions for further studies. In Fig. 7, the illuminance from ambient light in the visible range is set to its maximum value ($E_{\text{v,ab,vr}} = 52622$ lux). The mean cell data rate increases up to a certain point and then degrades, because the larger the bandwidth, the higher the receiver noise becomes according to (18). Besides, a larger bandwidth means that power is wasted on subcarriers which are highly attenuated. Thus, each communication setup is configured at the optimal W value that maximizes the average data rate. The maximum capacity of DCO-OFDM is
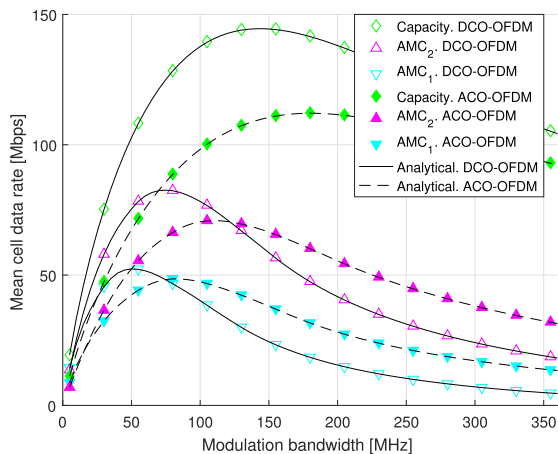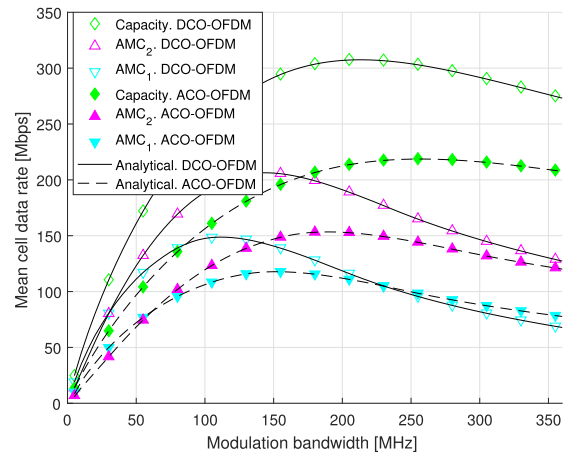

FIGURE 8. Average data rate *s* vs. bandwidth *W* at capacity, with AMC$_1$ and AMC$_2$, at night ($E_{\text{v,ab,vr}} = 0$ lux).

144.5 Mbps, which is obtained for $W = 140$ MHz; AMC$_1$ achieves a maximum of 52.37 Mbps for $W = 50$ MHz; and AMC$_2$ operates at 82.59 Mbps at $W = 75$ MHz. However, although ACO-OFDM exhibits a better SNR performance than DCO-OFDM, since ACO-OFDM uses half of the FD subcarriers of DCO-OFDM, the resultant achievable average data rate is lower. The maximum average data rates obtained by ACO-OFDM are 112.10, 48.53 and 70.89 Mbps for W values of 180, 80 and 110 MHz, at capacity, using AMC$_1$ and AMC$_2$, respectively. During the night (Fig. 8) the background light disappears, which results in a considerable reduction of the shot noise. In this case, the increased modulation bandwidth is not so detrimental and, as a consequence, the achievable mean cell data rates are much higher than during the daytime.

Observe in Fig. 7 and Fig. 8 that ACO-OFDM provides a better performance than DCO-OFDM for W values beyond a cross-over point, where the reduction in the noise achieved by ACO-OFDM becomes more important than using more FD subcarriers for carrying information.

Fig. 9 shows that the uncoded QAM scheme AMC$_1$ exhibits a high outage probability in comparison to AMC$_2$. The analytical outage probability is computed as $F_{\Gamma|k=1}(\gamma_{\min})$ in (32). Note that the larger the bandwidth, the higher the noise becomes and, as a consequence, the
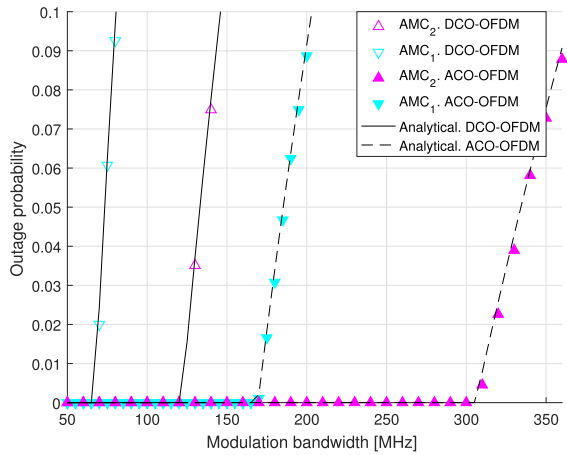

FIGURE 7. Average data rate *s* vs. bandwidth *W* at capacity, with AMC$_1$ and AMC$_2$, during daytime ($E_{\text{v,ab,vr}} = 52622$ lux).

FIGURE 9. Outage probability vs. modulation bandwidth W with AMC_1 and AMC_2, during daytime ($E_{v,ab,vr} = 52622$ lux).
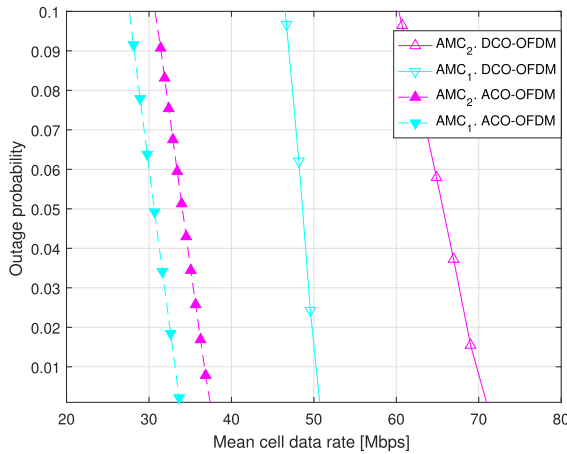

FIGURE 10. Outage probability vs. mean cell data rate with AMC_1 and AMC_2, during daytime ($E_{v,ab,vr} = 52622$ lux).

FIGURE 11. Optimal modulation bandwidth for maximizing the average data rate throughout the day.

FIGURE 12. Achievable maximal average data rate throughout the day.

outage probability increases. Generally DCO-OFDM suffers from a much higher outage probability than ACO-OFDM, because the SNR performance of ACO-OFDM is better, as seen in Fig. 6. An outage probability of 10% at most is shown in Fig. 9 because larger outage probabilities are not interesting for practical systems. Note that the degradation is not as gradual as expected because the working SINR regions are low for all modulation bandwidths due to the high shot noise produced during daytime ($E_{v,ab,vr} = 52622$ lux). In our future research we will use adaptive layered ACO-OFDM (LACO-OFDM) for avoiding the avalanche-like outage probability degradation imposed by the excessive shot noise inflicted by intense sunshine [40].

Fig. 10 shows the relation between the mean cell data rate and the outage probability. A higher outage probability involves a higher modulation bandwidth, as seen in Fig. 9. Higher mean cell data rates can be achieved for very low values of outage probability, as shown in Fig. 7 and Fig. 9. As expected, DCO-OFDM is more efficient than ACO-OFDM because, for the same outage probability,
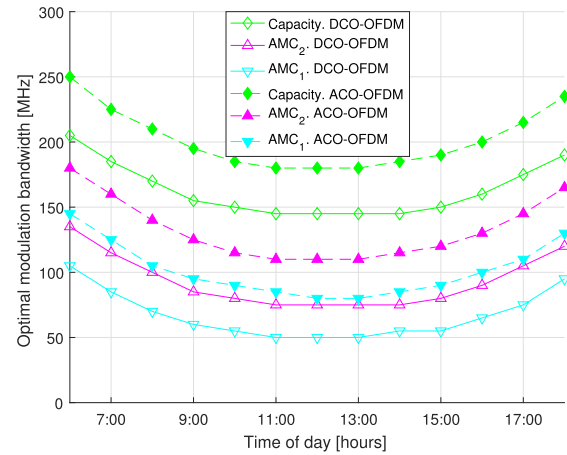
the achieved mean cell data rate is higher even when using a lower modulation bandwidth.

It has been demonstrated in Fig. 7, Fig. 8 and Section III-B that an optimal W can be found by maximizing the average data rate for certain conditions. It is interesting to study how these optimal W and average data rates vary during the day. Fig. 11 shows the optimal modulation bandwidth for certain hours of the day that makes the maximal average data rate represented in Fig. 12 possible. As expected, noon is the most critical time, when the lowest average data rate is obtained in bright sunshine. However, a reasonable value of 83 Mbps can still be achieved, when DCO-OFDM and AMC_2 are used. Higher average data rate values can be obtained by more spectrally efficient schemes than the uncoded QAM (AMC_1), such as AMC_2. In general, DCO-OFDM outperforms ACO-OFDM. Nevertheless, the higher the background noise power, the lower the differences between DCO-OFDM and ACO-OFDM become.

V. CONCLUSION
This paper presented the first analytical study of O-OFDM in outdoor VLC scenarios. The modulation bandwidth

adaptation results in substantial data rate and outage probability improvements. The background noise increases with the modulation bandwidth, hence the optimum sampling frequencies and bandwidths were found for specific environmental conditions.

Although ACO-OFDM can perform at higher modulation bandwidths than DCO-OFDM for the same outage probability, DCO-OFDM provides better performance in terms of mean cell data rate. Generally, DCO-OFDM achieves a better performance than ACO-OFDM in the absence of background noise than during the daytime. For the practical employment of VLC schemes in outdoor scenarios, more robust schemes relying on strong forward error correction-aided (FEC-aided) automatic repeat request (ARQ) schemes and power-efficient modulation arrangements have to be developed, using for example M-ary orthogonal modulation.

APPENDIX
Demonstration of limits for the average data rate:

1) SHANNON LIMIT

$$s(W) = \frac{W}{K} \sum_{k \in \mathcal{K}_*} \int_h^{\sqrt{h^2 + \tilde{R}^2}} \log_2\left(1 + \Gamma(k, d, W)\right) f_D(d)\, \mathrm{d}d, \quad (37)$$

where $\Gamma(k, d, W)$ is represented in (21) as

$$\Gamma(k, d, W) = \frac{C_1}{C_4 + \left(C_2 \cdot d^\alpha + C_3 \cdot d^{2\alpha}\right) \cdot W \cdot \exp\left(\frac{kW}{KF_{\mathrm{fe}}}\right)}, \quad (38)$$

where we have $\lim_{W \to \infty} \Gamma(k, d, W) = 0$ and it decreases exponentially, thus $\lim_{W \to \infty} s(W) = 0$. Furthermore, $\lim_{W \to 0} \Gamma(k, d, W) = \frac{C_1}{C_4}$ which is a constant and $\lim_{W \to 0} s(W) = 0$.

2) AMC SCHEMES

$$s(W) = \frac{W}{K} \sum_{k \in \mathcal{K}_*} \sum_{n=1}^{N} \epsilon[n]$$
$$\times \left(\frac{d_{\mathrm{th}}\left(\gamma_{\mathrm{th}}[n], W, k\right)^2 - d_{\mathrm{th}}\left(\gamma_{\mathrm{th}}[n+1], W, k\right)^2}{\tilde{R}^2}\right), \quad (39)$$

where

$$d_{\mathrm{th}}(\gamma_{\mathrm{th}}, W, k)$$
$$= \left(\frac{-C_2}{2C_3} + \sqrt{\left(\frac{C_2}{2C_3}\right)^2 + \frac{C_1 - C_4 \gamma_{\mathrm{th}}}{C_3 W \exp\left(\frac{kW}{KF_{\mathrm{fe}}}\right) \gamma_{\mathrm{th}}}}\right)^{1/\alpha}. \quad (40)$$

Calculating $\lim_{W \to \infty} d_{\mathrm{th}}(\gamma_{\mathrm{th}}, W, k) = 0$, then $\lim_{W \to \infty} s(W) = 0$. Also, $\lim_{W \to 0} s(W) = 0$ because the order of W is higher than the order of $W^{1/\alpha}$ ($\alpha = m + 3 > 3$).

REFERENCES

[1] L. Hanzo, H. Haas, S. Imre, D. O'Brien, M. Rupp, and L. Gyongyosi, "Wireless myths, realities, and futures: From 3G/4G to optical and quantum wireless," *Proc. IEEE*, vol. 100, no. Special Centennial Issue, pp. 1853–1888, May 2012.

[2] T. S. Rappaport *et al.*, "Millimeter wave mobile communications for 5G cellular: It will work!" *IEEE Access*, vol. 1, pp. 335–349, 2013.

[3] T. Komine and M. Nakagawa, "Fundamental analysis for visible-light communication system using LED lights," *IEEE Trans. Consum. Electron.*, vol. 50, no. 1, pp. 100–107, Feb. 2004.

[4] D. Tsonev, S. Videv, and H. Haas, "Towards a 100 Gb/s visible light wireless access network," *Opt. Express*, vol. 23, no. 2, pp. 1627–1637, Jan. 2015.

[5] R. Zhang, J. Wang, Z. Wang, Z. Xu, C. Zhao, and L. Hanzo, "Visible light communications in heterogeneous networks: Paving the way for user-centric design," *IEEE Wireless Commun.*, vol. 22, no. 2, pp. 8–16, Apr. 2015.

[6] X. Li, F. Jin, R. Zhang, J. Wang, Z. Xu, and L. Hanzo, "Users first: User-centric cluster formation for interference-mitigation in visible-light networks," *IEEE Trans. Wireless Commun.*, vol. 15, no. 1, pp. 39–53, Jan. 2016.

[7] Y. Wang, X. Wu, and H. Haas, "Load balancing game with shadowing effect for indoor hybrid LiFi/RF networks," *IEEE Trans. Wireless Commun.*, vol. 16, no. 4, pp. 2366–2378, Apr. 2017.

[8] J. Wang, C. Jiang, H. Zhang, X. Zhang, V. C. M. Leung, and L. Hanzo, "Learning-aided network association for hybrid indoor LiFi-WiFi systems," *IEEE Trans. Veh. Technol.*, vol. 67, no. 4, pp. 3561–3574, Apr. 2018.

[9] X. Li, R. Zhang, and L. Hanzo, "Cooperative load balancing in hybrid visible light communications and WiFi," *IEEE Trans. Commun.*, vol. 63, no. 4, pp. 1319–1329, Apr. 2015.

[10] W.-T. Shaw *et al.*, "Hybrid architecture and integrated routing in a scalable optical–wireless access network," *J. Lightw. Technol.*, vol. 25, no. 11, pp. 3443–3451, Nov. 2007.

[11] F. Fidler, M. Knapek, J. Horwath, and W. R. Leeb, "Optical communications for high-altitude platforms," *IEEE J. Sel. Topics Quantum Electron.*, vol. 16, no. 5, pp. 1058–1070, Sep./Oct. 2010.

[12] L. Yang, M. O. Hasna, and X. Gao, "Performance of mixed RF/FSO with variable gain over generalized atmospheric turbulence channels," *IEEE J. Sel. Areas Commun.*, vol. 33, no. 9, pp. 1913–1924, Sep. 2015.

[13] Z.-G. Sun, H. Yu, and Y.-J. Zhu, "A superimposed relaying strategy and power allocation for outdoor visible light communications," *IEEE Access*, vol. 5, pp. 9555–9561, 2017.

[14] M. Uysal, Z. Ghassemlooy, A. Bekkali, A. Kadri, and H. Menouar, "Visible light communication for vehicular networking: Performance study of a V2V system using a measured headlamp beam pattern model," *IEEE Veh. Technol. Mag.*, vol. 10, no. 4, pp. 45–53, Dec. 2015.

[15] S. J. Lee, J. K. Kwon, S. Y. Jung, and Y. H. Kwon, "Simulation modeling of visible light communication channel for automotive applications," in *Proc. Int. IEEE Conf. Intell. Transp. Syst.*, Sep. 2012, pp. 463–468.

[16] A. M. Căilean and M. Dimian, "Current challenges for visible light communications usage in vehicle applications: A survey," *IEEE Commun. Surveys Tuts.*, vol. 19, no. 4, pp. 2681–2703, 4th Quart., 2017.

[17] Y. H. Chung and S.-B. Oh, "Efficient optical filtering for outdoor visible light communications in the presence of sunlight or articifical light," in *Proc. Int. Symp. Intell. Signal Process. Commun. Syst.*, Nov. 2013, pp. 749–752.

[18] I. E. Lee, M. L. Sim, and F. W. L. Kung, "Performance enhancement of outdoor visible-light communication system using selective combining receiver," *IET Optoelectron.*, vol. 3, no. 1, pp. 30–39, Feb. 2009.

[19] M. Kinoshita *et al.*, "Motion modeling of mobile transmitter for image sensor based I2V-VLC, V2I-VLC, and V2V-VLC," in *Proc. IEEE Globecom Workshops*, Dec. 2014, pp. 450–455.

[20] F. Knobloch, "Channel gain and frame error rate for optical street lighting communication," in *Proc. Int. Conf. Telecommun.*, Jul. 2015, pp. 1–5.

[21] M. S. Islim *et al.*, "The impact of solar irradiance on visible light communications," *J. Lightw. Technol.*, vol. 36, no. 12, pp. 2376–2386, Jun. 15, 2018.

[22] J. Armstrong, "OFDM for optical communications," *J. Lightw. Technol.*, vol. 27, no. 3, pp. 189–204, Feb. 1, 2009.

[23] H. Le Minh *et al.*, "100-Mb/s NRZ visible light communications using a postequalized white LED," *IEEE Photon. Technol. Lett.*, vol. 21, no. 15, pp. 1063–1065, Aug. 1, 2009.

[24] J. M. Kahn and J. R. Barry, "Wireless infrared communications," *Proc. IEEE*, vol. 85, no. 2, pp. 265–298, Feb. 1997.

[25] H. Elgala, R. Mesleh, and H. Haas, "Practical considerations for indoor wireless optical system implementation using OFDM," in *Proc. Int. Conf. Telecommun.*, Jun. 2009, pp. 25–29.

[26] H. Elgala, R. Mesleh, and H. Haas, "Non-linearity effects and predistortion in optical OFDM wireless transmission using LEDs," *Int. J. Ultra Wideband Commun. Syst.*, vol. 1, no. 2, pp. 143–150, Oct. 2009.

[27] B. G. Guzmán and V. P. G. Jiménez, "DCO-OFDM signals with derated power for visible light communications using an optimized adaptive network-based fuzzy inference system," *IEEE Trans. Commun.*, vol. 65, no. 10, pp. 4371–4381, Oct. 2017.

[28] B. G. Guzmán, A. A. Dowhuszko, V. P. G. Jiménez, and A. I. Pérez-Neira, "Robust cooperative multicarrier transmission scheme for optical wireless cellular networks," *IEEE Photon. Technol. Lett.*, vol. 30, no. 2, pp. 197–200, Jan. 15, 2018.

[29] B. G. Guzmán, A. L. Serrano, and V. P. G. Jiménez, "Cooperative optical wireless transmission for improving performance in indoor scenarios for visible light communications," *IEEE Trans. Consum. Electron.*, vol. 61, no. 4, pp. 393–401, Nov. 2015.

[30] S. Dimitrov, S. Sinanovic, and H. Haas, "Clipping noise in OFDM-based optical wireless communication systems," *IEEE Trans. Commun.*, vol. 60, no. 4, pp. 1072–1081, Apr. 2012.

[31] N. L. Johnson, S. Kotz, and N. Balakrishnan, *Continuous Univariate Distributions*, vol. 1, 2nd ed. Hoboken, NJ, USA: Wiley, 1994.

[32] D. Dardari, V. Tralli, and A. Vaccari, "A theoretical characterization of nonlinear distortion effects in OFDM systems," *IEEE Trans. Commun.*, vol. 48, no. 10, pp. 1755–1764, Oct. 2000.

[33] A. Goldsmith, *Wireless Communications*. New York, NY, USA: Cambridge Univ. Press, 2005.

[34] A. M. Khalid, G. Cossu, R. Corsini, P. Choudhury, and E. Ciaramella, "1-Gb/s transmission over a phosphorescent white LED by using rate-adaptive discrete multitone modulation," *IEEE Photon. J.*, vol. 4, no. 5, pp. 1465–1473, Oct. 2012.

[35] R. E. Bird and C. Riordan, "Simple solar spectral model for direct and diffuse irradiance on horizontal and tilted planes at the Earth's surface for cloudless atmospheres," *J. Climate Appl. Meteorol.*, vol. 25, no. 1, pp. 87–97, 1986.

[36] R. Rondanelli, A. Molina, and M. Falvey, "The Atacama surface solar maximum," *Bull. Amer. Meteorol. Soc.*, vol. 96, no. 3, pp. 405–418, 2015.

[37] H. Jin, S. Jin, L. Chen, S. Cen, and K. Yuan, "Research on the lighting performance of LED street lights with different color temperatures," *IEEE Photon. J.*, vol. 7, no. 6, pp. 1–9, Dec. 2015.

[38] F. Xiong, *Digital Modulation Techniques*, 2nd ed. Norwood, MA, USA: Artech House, 2006.

[39] S. Webster, "Designing an LTE network using EDX SignalPro," *EDX Wireless, Technol. White Paper*, Sep. 2010, pp. 1–12.

[40] X. Zhang, Q. Wang, R. Zhang, S. Chen, and L. Hanzo, "Performance analysis of layered ACO-OFDM," *IEEE Access*, vol. 5, pp. 18366–18381, 2017.

BORJA GENOVÉS GUZMÁN (S'14) received the B.Sc. degree and the M.Sc. degree (Hons.) from the Universidad Carlos III de Madrid in 2013 and 2015, respectively, and the M.Sc. degree in electrical engineering from the Institut Mines-Télécom, France, in 2015. He is currently pursuing the Ph.D. degree with the Communications Research Group, Universidad Carlos III de Madrid. He was a Visiting Scholar with the Southampton Wireless Group, The University of Southampton, and the LiFi Research and Development Centre, The University of Edinburgh, in 2017 and 2018, respectively. He has participated in several national and European projects. His current research focuses on new techniques to improve the efficiency of optical wireless communications systems. He received the First Prize in Graduation National Awards from the Ministry of Education, Culture and Sports of Spain. He was a recipient of the FPU Scholarship from the Spanish Ministry of Education, Culture and Sports of Spain.

VÍCTOR P. GIL JIMÉNEZ (S'00–AM'02–M'03–SM'12) received the B.S. degree in telecommunication in telecommunication from the University of Alcalá in 1998 and the M.S. degree in telecommunication and the Ph.D. degree from the Universidad Carlos III de Madrid in 2001 and 2005, respectively. He is currently an Associate Professor with the Department of Signal Theory and Communications, Universidad Carlos III de Madrid. He was a Communications Staff with the Spanish Antarctica Base in 1999. He visited the University of Leeds, U.K., in 2003, the Chalmers University of Technology, Sweden, in 2004, and the Instituto de Telecommunicaçoes, Portugal, from 2008 to 2010. He has also led several private and national Spanish projects and has participated in several European and international projects. He holds one patent. His interests are in the field of the advanced multicarrier systems for wireless radio and visible light communications. He has received the Master Thesis and the Ph.D. Thesis Award from the Professional Association of Telecommunication Engineers of Spain in 1998 and 2006, respectively. He held the IEEE Spanish Communications and Signal Processing Joint Chapter Chair from 2015 to 2018.

MARI CARMEN AGUAYO-TORRES received the M.S. degree and the Ph.D. degree in telecommunication engineering from the University of Malaga, Spain, in 1994 and 2001, respectively. Her Ph.D. thesis was on adaptive OFDM. She is currently a Professor with the Department of Communications Engineering, University of Málaga. Her main research interests are 5G technologies with probabilistic QoS guarantees. Her current work includes theoretical analysis with tools such as stochastic geometry besides statistical evaluation of real and simulated networks. She is involved in a number of public and private funded projects and actively collaborates with industry, mainly in the field of wireless communications.

HARALD HAAS (S'98–AM'00–M'03–SM'16–F'17) received the Ph.D. degree from The University of Edinburgh in 2001. He is currently the Chair of Mobile Communications with The University of Edinburgh. He is the Initiator, a Co-Founder, and the Chief Scientific Officer of pureLiFi Ltd., and the Director of the LiFi Research and Development Centre, The University of Edinburgh. He has authored 430 conference and journal papers, including a paper in science and co-authored a book *Principles of LED Light Communications Towards Networked Li-Fi* (Cambridge University Press, 2015). His main research interests are in optical wireless communications, hybrid optical wireless and RF communications, spatial modulation, and interference coordination in wireless networks. He first introduced and coined spatial modulation and LiFi. LiFi was listed among the 50 best inventions in *TIME Magazine* in 2011. He was elected as a fellow of the Royal Society of Edinburgh in 2017. In 2012 and 2017, he was a recipient of the prestigious Established Career Fellowship from the Engineering and Physical Sciences Research Council (EPSRC) within Information and Communications Technology in the U.K. In 2014, he was selected by EPSRC as one of 10 Recognizing Inspirational Scientists and Engineers Leaders in the U.K. He was a co-recipient of the EURASIP Best Paper Award for the *Journal on Wireless Communications and Networking* in 2015 and the Jack Neubauer Memorial Award of the IEEE Vehicular Technology Society. In 2016, he received the Outstanding Achievement Award from the International Solid State Lighting Alliance. He was a co-recipient of recent best paper awards at VTC 2013, VTC 2015, ICC 2016, ICC 2017, and ICC 2018. He is an Editor of the IEEE TRANSACTIONS ON COMMUNICATIONS and the IEEE JOURNAL OF LIGHTWAVE TECHNOLOGIES. He was an invited speaker at TED Global 2011, and his talk on Wireless Data from Every Light Bulb has been watched online over 2.4 million times. He gave a second TED Global lecture in 2015 on the use of solar cells as LiFi data detectors and energy harvesters. This has been viewed online over 2 million times.

LAJOS HANZO (M'91–SM'92–F'04) received the D.Sc. degree in electronics in 1976 and the Ph.D. in 1983. During his 40-year career in telecommunications, he has held various research and academic posts in Hungary, Germany, and U.K. Since 1986, he has been with the School of Electronics and Computer Science, University of Southampton, U.K. He is currently directing a academic research team, working on a range of research projects in the field of wireless multimedia communications sponsored by industry, the Engineering and Physical Sciences Research Council, U.K., the European Research Council's Advanced Fellow Grant, and the Royal Society's Wolfson Research Merit Award. He is an enthusiastic supporter of industrial and academic liaison and he offers a range of industrial courses. He has successfully supervised 111 Ph.D. students, co-authored 18 John Wiley/IEEE Press books on mobile radio communications totaling in excess of 10 000 pages, published over 1700 research contributions at the IEEE Xplore. He received an Honorary Doctorate from the Technical University of Budapest in 2009 and The University of Edinburgh in 2015. In 2016, he was admitted to the Hungarian Academy of Science. He is a Governor of the IEEE VTS. He served as the TPC Chair and the General Chair of the IEEE conferences, presented keynote lectures and has been awarded a number of distinctions. He is the Chair in telecommunications with the University of Southampton. From 2008 to 2012, he was an Editor-in-Chief of the IEEE Press and a Chaired Professor at Tsinghua University, Beijing. He has over 33 000 citations. For further information on research in progress and associated publications please refer to http://www-mobile.ecs.soton.ac.uk.

• • •